Hydrol. Earth Syst. Sci. Discuss., 12, 12089–12120, 2015
www.hydrol-earth-syst-sci-discuss.net/12/12089/2015/
doi:10.5194/hessd-12-12089-2015

Hydrology and Earth System Sciences Discussions
Open Access

Macropore flow at the field scale: predictive performance of empirical models and X-ray CT analyzed macropore characteristics

M. Naveed[1], P. Moldrup[3], M. Schaap[4], M. Tuller[4], R. Kulkarni[5], H.-J. Vögel[6], and L. Wollesen de Jonge[2]

[1]Institute of Environmental and Biological Sciences, University of Aberdeen, King's College, Aberdeen, AB24 3FX, UK
[2]Department of Agroecology, Faculty of Science and Technology, Aarhus University, Blichers Allé 20, Postbox 50, 8830 Tjele, Denmark
[3]Department of Civil Engineering, Aalborg University, Sohngaardsholmsvej 57, 9000 Aalborg, Denmark
[4]Department of Soil, Water and Environmental Science, The University of Arizona, 1177 E. 4th Street, Tucson, AZ 85721, USA
[5]Department of Electrical and Computer Engineering, The University of Arizona, 1177 E. 4th Street, Tucson, AZ 85721, USA
[6]Department of Soil Physics, Helmholtz Center for Environmental Research-UFZ, Theodor-Lieser-Straße 4, 06120 Halle (Saale), Germany

Received: 21 October 2015 – Accepted: 31 October 2015 – Published: 20 November 2015

Correspondence to: M. Naveed (muhammad.naveed@abdn.ac.uk)

Published by Copernicus Publications on behalf of the European Geosciences Union.

Abstract

Predictions of macropore flow is important for maintaining both soil and water quality as it governs key related soil processes e.g. soil erosion and subsurface transport of pollutants. However, macropore flow currently cannot be reliably predicted at the field scale because of inherently large spatial variability. The aim of this study was to perform field scale characterization of macropore flow and investigate the predictive performance of (1) current empirical models for both water and air flow, and (2) X-ray CT derived macropore network characteristics. For this purpose, 65 cylindrical soil columns (6 cm diameter and 3.5 cm height) were extracted from the topsoil (5 to 8.5 cm depth) in a 15 m × 15 m grid from an agricultural loamy field located in Silstrup, Denmark. All soil columns were scanned with an industrial CT scanner (129 µm resolution) and later used for measurements of saturated water permeability, air permeability and gas diffusivity at −30 and −100 cm matric potentials. Distribution maps for both water and air permeabilities and gas diffusivity reflected no spatial correlation irrespective of the soil texture and organic matter maps. Empirical predictive models for both water and air permeabilities showed poor performance as they were not able to realistically capture macropore flow because of poor correlations with soil texture and bulk density. The tested empirical model predicted well gas diffusivity at −100 cm matric potential, but relatively failed at −30 cm matric potential particularly for samples with biopore flow. Image segmentation output of the four employed methods was nearly the same, and matched well with measured air-filled porosity at −30 cm matric potential. Many of the CT derived macropore network characteristics were strongly interrelated. Most of the macropore network characteristics were also strongly correlated with saturated water permeability, air permeability, and gas diffusivity. The correlations between macropore network characteristics and macropore flow parameters were further improved on dividing soil samples into samples with biopore and matrix flow. Observed strong correlations between macropore network characteristics and macropore flow highlighted the

HESSD

12, 12089–12120, 2015

need of further research on numerical simulations of macropore flow based on X-ray CT images. This could pave the way for the digital soil physics laboratory in the future.

1 Introduction

The effect of macropore flow on partitioning of precipitation between runoff and infiltration, on plant water uptake and plant growth, on biogeochemical cycling rates, and on the potential risk of ground water contamination is widely recognized (Iversen et al., 2011; de Jonge et al., 2004; Fox et al., 2004; Moustafa, 2000). Thus, over the last decade major research efforts have been devoted to improve the understanding of macropore flow processes and their governing parameters, and to develop predictive macropore flow models (Jarvis, 2007). Macropore flow and transport refers to the localized and usually rapid movement of water and solutes through soils. Macropores resulting from biological activity (root channels, worm holes etc.), geological forces (subsurface erosion, shrinkage and swelling etc.), and agricultural management practices (e.g. plowing) serve as the main channels for this rapid and long-distance flow and transport of water, air, and contaminants. Macropore flow is largely determined by soil structure and is generally a dominating process in loamy and clayey soils (Jarvis et al., 2009) where large inter-aggregate pores and biopores often act as pathways for rapid flow and transport. The transition from matrix to macropore flow (equilibrium to non-equilibrium) depends on the pore size and continuity, and the degree of soil saturation (Bouma, 1981). Macropore flow often occurs in pores with equivalent effective cylindrical diameters larger than 0.3–0.5 mm, which means that the water potential needs to be close to zero and the water content close to saturation for these pores to be activated (Jarvis, 2007).

Soil and crop management practices strongly modify soil structure and thus the extent of macropore flow and transport. Wang et al. (2013) and Gonzalez-Sosa et al. (2010) studied the impact of land use on the hydraulic properties of the topsoil on the Loess Plateau of China and suburban catchment of France, respectively. Both studies have reported higher saturated hydraulic conductivity values for forestland, intermediate for permanent pasture, and lower for farmland soils. This is primarily due to the large presence of biota and less disturbance in forests and permanent pastures as compared to cultivated lands (Naveed et al., 2014a; Norgaard et al., 2013; Pérèsa et al., 2012). Application of animal manure and fertilizers can also influence macropore flow by first altering soil structure and second by promoting the density of the earthworms, particularly deep penetrating anecic worms (Naveed et al., 2014b). Climatic conditions (seasonal temperature and precipitation variations) might also affect soil structure and macropore flow through interactions with physical processes such as cyclic freezing/thawing and wetting/drying (Hu et al., 2012). Due to the complex interrelations and the significant number of influencing factors, a large spatial variability of saturated hydraulic conductivity has been reported for different regions of the world (Wang et al., 2013; Raczkowski et al., 2012; Iversen et al., 2011). Therefore, the predictive capabilities of empirical models/pedotransfer functions for saturated water permeability are limited because they ignore the effects of key site factors and underestimate the significance of soil structure (Vereecken et al., 2010). Recently, pedotransfer functions for saturated hydraulic conductivity that account for soil structure have been developed, but they are rarely applied due to the complexity of input parameters and the still relatively significant prediction inaccuracies (Jarvis et al., 2013; Iversen et al., 2011; Lilly et al., 2008).

Along with prediction of macropore water flow (i.e. saturated water permeability), prediction of macropore air flow (i.e. air permeability and diffusivity) is also important. Air permeability is a key parameter in the design of soil vapor extraction technique. Air diffusivity is of importance because the availability of oxygen to plant roots via diffusion phenomena is a basic factor of soil productivity. Various empirical models have been proposed in the past for the prediction of air permeability (Deepagoda et al., 2011; Kawamoto et al., 2006) and air diffusivity (Deepagoda et al., 2011; Moldrup et al., 2000). However, none of the study has tested their application on the field scale yet.

HESSD
12, 12089–12120, 2015

Developments of new imaging techniques allow not only visual observation but also quantification of pore network complexity. Application of X-ray Computed Tomography (CT) provides emerging alternative means for estimating subsurface macropore flow and transport (Wildenschild and Sheppard, 2013). Over the last decade, various studies on the characterization of macropore structure (macroporosity, macropore size distribution, volume, surface area, tortuosity etc.) were conducted for different land use and management systems with X-ray CT (Larsbo et al., 2014; Hu et al., 2014; Naveed et al., 2013; Vogel et al., 2010; Luo et al., 2010). However, only a few studies to date were published on quantitatively relating macropore network characteristics to the observations of macropore flow. Larsbo et al. (2014) reported significant correlations between X-ray CT derived macropore network characteristics and flow and transport parameters. Paradelo et al. (2013) found that X-ray CT derived macroporosity was strongly correlated with saturated hydraulic conductivity, solute dispersivity, arrival time, and contaminant breakthrough. Luo et al. (2010) reported that macroporosity, path number, hydraulic radius, and macropore angle were the most useful X-ray CT derived parameters for predicting macropore flow and transport under saturated conditions. These studies were based on a limited number of soil samples due to high expenses of X-ray CT scanning, and none of them was on the field scale. In-continuation with this research a comprehensive field scale study was carried out with the following specific objectives:

1. How does the spatial variability of macropore water and air flow correlate with the spatial variability of soil texture and organic matter content at the field scale?

2. Are traditional empirical models able to predict macropore water and air flow at the field scale?

3. Which X-ray CT derived macropore network characteristics are most useful for predicting macropore water and air flow at the field scale?

HESSD
12, 12089–12120, 2015

2 Materials and methods

2.1 Study site and soil sampling

The 1.69 ha study site located in Silstrup in northwestern Denmark (56°55′56″ N, 8°38′44″ E) is covered with glacial till, a dominant geological formation covering about 43 % of all farmland in Denmark (Geological Survey of Denmark and Greenland, 1999). The top meter of the soil is highly fractured and bioturbated, containing 100 to 1000 biopores per m^2. The field has not been tilled for about 3 years prior to soil sampling. The field has been plowed in December 2008 to 23 cm depth and harrowed twice to 5 cm depth in March 2009. Since then the soil was only disturbed when slurry was injected in 10 cm depth in April 2009 and in 4 to 5 cm depth in September 2009. A thorough overview of management practices performed at the study site between 2006 and 2010 is provided in Norgaard et al. (2013).

65 undisturbed cylindrical soil cores (6 cm ID and 3.5 cm height) were extracted from the topsoil (5 to 8.5 cm depth) in summer 2012. At the time of sampling the field was cultivated with red fescue (*Festuca rubra* L.). The soil columns were sampled on a rectangular 15 m by 15 m grid (Fig. 1). All soil columns were extracted by stepwise pushing a customized core sampler containing the aluminum sampling cylinders into the soil and step by step removing the surrounding material. Extracted soil columns were immediately covered with tight plastic lids, placed in plastic bags, and carefully transported from field to the laboratory to avoid smearing and compaction effects. In the laboratory the soil columns were preserved at −2 °C until measurements started. In addition, bulk soil samples were collected from each point at the same soil depth for texture and organic carbon analysis.

2.2 X-ray computed tomography scanning and analysis

An industrial X-Ray CT scanner (X-Tek HMX225) at the Helmholtz Center for Environmental Research in Halle in Germany was used to scan the intact soil columns at an energy level of 180 kV and a current of 400 µA. A copper filter was placed between the X-ray source and the soil column to alleviate beam hardening. The shadow projections (radiographs) were reconstructed with a Feldkamp cone-beam algorithm (Feldkamp et al., 1984) to obtain 16-bit grayscale 3-D data comprised of 500×500×300 voxels (resolution is 129 µm). For subsequent analysis, the 3-D grayscale volumes were cropped to remove the container wall and disturbed regions on the top and bottom of the sample. Before the image segmentation, a 3-D median filter (Jassonge et al., 2007) with a radius of 6 voxels was applied to the grayscale volumes to remove noise. Though, median filtering is computationally more demanding than conventional smoothing filters, it is less sensitive to outlier values and thus preserve edges. Image segmentation was carried out with four different methods. Two of them were global segmentation methods proposed by Ridler and Calvard (1978) and Otsu (1979), which consider the global grayscale histogram of the entire cropped samples. The other two methods were locally adaptive segmentation methods developed by Sauvola and Pitenkien (2000) and Kulkarni et al. (2012), which separate individual voxel classes based on the information from the local voxel neighborhood. For the Sauvola and Pitenkien (2000) method, a radius of 25 voxels and a k value of 0.5 were used. Kulkarni et al. (2012) developed an image segmentation code based on Bayesian Markov Random Field (MRF) framework. The MRF model requires parameterization with a β value, which was set equal to 2.0 in this study. The MRF model was initialized using K-means clustering for selection of two seed regions (pore and solids) within the X-ray CT data.

The segmented images for each soil column obtained using Kulkarni et al. (2012) method were further analyzed to obtain macroporosity, connected macroporosity, minimum connected macroporosity, macropore specific surface area, macropore hydraulic radius, macropore mean diameter, macropore fractal dimension, macropore global connectivity, and macropore local connectivity with the Image-J software package (Rasband, 2011). The number of pore voxels was determined from the histogram of the segmented images, and macroporosity was then calculated as the ratio of the number of pore voxels to the number of total column voxels. The connected macro porosity was calculated based on only those pores, which were connected from top to bottom of the scanned and segmented core samples by removing all isolated pores. All isolated pores were removed with the Image-J plugin “Find Connected Regions”. Minimum connected macroporosity was defined and calculated as the minimum value of the connected macroporosity while moving voxel layer by voxel layer from the top to the bottom of the core. Macropore specific surface area was defined as the ratio of surface area of macropores to the volume of soil sample. It was calculated with the Image-J plugin “Analyze Particles”. Macropore hydraulic radius was defined as the ratio of macropore volume and macropore surface area. It was also calculated with the Image-J plugin “Analyze Particles”. The macropore mean diameter was estimated with a local 3-D thickness algorithm proposed by Dougherty and Kunzelmann (2007) and embedded in the Image-J plugin “Bone-J”. This algorithm defines the pore diameter as the diameter of the largest sphere that fits within the pore. The histogram of the thickness map was used for estimating macropore size distribution and macropore mean diameter. Macropore fractal dimension was calculated as a measure of the heterogeneity of the spatial distribution of macroporosity with the Image-J plugin “Bone-J”. Macropore global connectivity was defined and calculated the ratio of volume of macropores connected from top to bottom of soil column to the total macropore volume of soil column. The macropore local connectivity (MPLC) was estimated with the Image J plugin “Bone-J”, and defined as:

$$\text{MPLC} = -E/V, \quad E = N - C + H \tag{1}$$

where E is Euler number, V is the volume of the soil column, N is the total number of disconnected macropore clusters that is equal to 1 here as MPLC was calculated based on the largest connected macropore cluster present in the soil column, C is the total number of redundant connections, and H is the total number of holes or cavities. A redundant connection can be cut without creating an additional isolated macropore cluster, and a hole can be an aggregate completely surrounded by pore space. Generally, a decreasing E indicates increasing macropore connectivity of the soil column.

HESSD
12, 12089–12120, 2015

2.3 Soil physical measurements

Soil texture was determined on disturbed samples that were passed through a 2 mm sieve with a combination of wet sieving and hydrometer methods. Soil organic carbon was determined with a LECO carbon analyzer (St. Joseph, MI, USA) coupled with an infrared CO_2 detector. A multiplication factor of 1.72 was used for converting soil organic carbon to soil organic matter. After X-ray CT scanning, air permeability and gas diffusivity at −30 and −100 cm matric potentials, and saturated hydraulic conductivity were measured on the same columns in the laboratory. The soil columns were placed in a sand box and saturated with water from the bottom. After saturation, suction was successively applied to establish matric potentials −30 and −100 cm. Air permeability (k_a) was then measured with the steady state method described in Iversen et al. (2001) both at −30 and −100 cm matric potentials. The pressure gradient was established at 5 hPa as frequently assumed pressure for the laminar flow during the measurements. The k_a was calculated from Darcy's equation based on the pressure difference across the core:

$$Q = \frac{k_a \Delta p a_s}{\eta_a L_s} \quad (2)$$

where Q ($L^3 T^{-1}$) is the volumetric flow rate, k_a (L^2) is air permeability, Δp (L) is the pressure difference across the column, η ($M L^{-1} T^{-1}$) is dynamic viscosity of air, a_s (L^2) is the cross-sectional area and L_s (L) is the length of the column. Gas diffusivities (D_P/D_0) at −30 and −100 cm matric potentials were measured with the one-chamber method described in Schjønning et al. (2013).

After that, the soil columns were resaturated, and the saturated hydraulic conductivity was measured with the constant head method (Klute and Dirksen, 1986). The laboratory measured saturated hydraulic conductivities were then converted to saturated water permeability at 20 °C:

HESSD
12, 12089–12120, 2015

$$k_w = k_{sat} \frac{\eta_w}{\rho_w g} \quad (3)$$

where k_w (L^2) is water permeability, k_{sat} ($L\,T^{-1}$) is saturated hydraulic conductivity, η_w ($M\,L^{-1}\,T^{-1}$) is dynamic viscosity of water, ρ_w ($M\,L^{-3}$) is density of water and g ($L\,T^{-2}$) is gravitational acceleration.

2.4 Statistics

Data collected for soil textural properties and macropore flow parameters were first subjected to classical statistical analysis to obtain descriptive statistics, including minimum, maximum, mean, median, SD, skewness, and coefficient of variation (CV). The degree of spatial variability of soil textural properties and macropore flow parameters was determined with ordinary kriging. The ArcMap 10.1 (Esri, Inc.) software was used to generate contour maps for each measured soil property. Spearman rank order correlation coefficients between macropore network characteristics and macropore flow parameters were calculated with the commercial SigmaPlot 11.0 software package. The correlations were considered significant if p values were below 0.01. Selected correlations were also graphically displayed and analyzed with linear or power regressions (that best described the data). The linear or power models were only fitted if they were significant at $p < 0.01$.

3 Results and discussion

3.1 Spatial variability of soil texture, organic matter, and macropore flow parameters

The soil of the study site was mainly classified as sandy loam (USDA-NRCS Web Soil Survey, 2010) with clay contents between 14 and 19 % and organic matter content varying from 2.9 to 3.8 % across the field. Descriptive statistics for all soil textural properties are depicted in Table 1. Clay and sand contents were positively skewed whereas silt and organic matter contents were negatively skewed. Although there was some skewness in soil textural properties, the mean and median values were quite similar. This indicated that the mean and median were not dominated by extreme values of the distributions. All soil textural properties were slightly variable across the field with coefficients of variation (CV) below 10 %. It has been reported in the literature that the CV for soil textural properties generally depends upon the extent of the study area. For example, Sharma et al. (2011) reported a CV for soil textural properties within the range of 20 to 30 % in a 40 ha agricultural field in New Mexico, while Wang et al. (2013) reported a CV within the range of 19 to 156 % across the Loess Plateau of China (620 000 km^2). Krigged maps indicated that soils with high clay contents were on the north side of field, whereas soils with high organic matter contents occupied the south side. Thus, clay and organic matter gradients run in opposite directions at the study site. Soils with high silt contents were on the eastern side of the field, whereas soils with high sand contents were on the western side (Fig. 1).

Descriptive statistics for saturated water permeability (k_w), air permeability (k_a), and gas diffusivity (D_P/D_0) at −30 and −100 cm matric potentials are provided in Table 1. Large positive skewness was observed for all five macropore flow parameters. Mean and median values were quite different, indicating that they were largely dominated by extreme values of the distribution. The k_w, k_a, and D_P/D_0 at −30 and −100 cm matric potentials showed the largest variations across the study site with a CV ranging from 92 to 218 %. High CV values were observed due to the presence of biopores in some of the soil columns, while not in others (marked samples in Fig. 1 are shown in Fig. 2). Irrespective of the extent of the study area, large variations in k_w were also reported in other studies (e.g. Wang et al., 2013; Sharma et al., 2011; Iqbal et al., 2005). Krigged maps for k_w, k_a, and D_P/D_0 look quite similar with some areas randomly exhibiting a high degree of macropore flow while matrix flow dominated in other regions

HESSD
12, 12089–12120, 2015

irrespective of soil texture and organic matter contents (Fig. 1). This is quite analogous to topography of a hilly area with some random peaks and low valleys.

3.2 Predictive performance of empirical models

For many hydrological applications, saturated water permeability (k_w) is estimated from more readily available proxy variables such as texture and bulk density. Various empirical models/pedotransfer functions (e.g. Iversen et al., 2011; Jarvis et al., 2009; Schaap et al., 2001; Wösten et al., 1999; Revil and Cathles, 1999) have been proposed in the past for predicting k_w. We have observed poor predictive performance of empirical models at the field scale for k_w for both models shown in Fig. 3 and also for those tested but not shown here such as Wösten et al. (1999), Vereecken et al. (1989), and Cosby et al. (1984). The primary reason is that empirical models/pedotransfer functions are based on soil texture and bulk density, and thus are not realistically able to capture macropore flow particularly for highly structured and bioturbated soils. Generally the empirical models over predicted k_w in case of matrix flow (unfilled symbols) while under predicted for soil columns with biopore flow (filled symbols). It should also be noted that permeability measurements on small samples as used in this study may not necessarily reflect the permeability at the scale of a soil horizon, for which the pedotransfer functions were developed.

Some efforts have also been made to develop empirical models for predicting air permeability (k_a) over the last decade (Moldrup et al., 1998; Kawamoto et al., 2006; Deepagoda et al., 2011). Among them, we have tested the predictive performance of the recently developed density-corrected k_a model (Deepagoda et al., 2011) as shown in Fig. 4a und b. The density-corrected k_a model performed reasonably well for soils with matrix flow, and comparatively fails for soils with higher k_a values for example in the presence of continuous structural cracks or biopores. Starting with Buckingham (1904) a more rigorous effort has been made in the past century to develop empirical models for prediction of gas diffusivity (Deepagoda et al., 2011). The tested WLR-Marshall model (Moldrup et al., 2000) reasonably predicted gas diffusivity for soil samples asso-

HESSD
12, 12089–12120, 2015

ciated with matrix flow and underestimated gas diffusivity for soil samples with biopore flow at −30 cm matric potential (Fig. 4c). This reflects that preferential diffusive flow could occur at higher matric potentials close to saturation even though gas diffusivity is a concentration-driven gas transport parameter. However at −100 cm matric potential, the WLR-Marshall model (Moldrup et al., 2000) predicted gas diffusivity well for all soil samples irrespective of matrix or biopore flow (Fig. 4d).

3.3 Correlations between macropore flow parameters and macropore network characteristics

All four employed image segmentation methods whether global or locally adaptive resulted into quite comparable macroporosity values (Fig. 5). This reflects that most of the image segmentation methods performed similarly when the X-Ray CT data quality is good with little partial volume effect, i.e. relatively clear pore and solid peaks of the histogram (Naveed, 2014). The obtained X-ray CT macroporosity based on the four investigated segmentation methods was plotted as a function of physically measured air-filled porosity at −30 cm matric potential (Fig. 5). The physically measured air-filled porosity at −30 cm matric potential agreed well with the X-ray CT analyzed macroporosity at 129 µm resolution. At −30 cm matric potential, all pores of diameter larger than 100 µm should have drained according to the Young Laplace capillary-rise equation. Referring to this, physically measured air-filled porosity at −30 cm matric potential (pores >100 µm) should be higher than the X-ray CT derived macroporosity (resolution = 129 µm). However, this is only true when assuming a parallel bundle of capillary tubes, which is clearly not realistic for natural soils. Due to the ink-bottle effect a considerable volume of pores > 100 µm are expected to be water filled after drainage at a water potential of −30 cm. Hence, no perfect match between the morphological pore size measured with CT and the hydraulic pore size estimated from the Young–Laplace equation can be expected (Vogel, 2000). Hence, the observed agreement between both measures is absolutely reasonable and confirms the accuracy of the employed image segmentation methods (Fig. 5). However, it must be noted that different image

HESSD
12, 12089–12120, 2015

segmentation methods can result in quite different macroporosity values if image quality is not good, i.e. lot of noise and partial volume effect as shown in Naveed (2014).

Spearman rank order correlation analysis between macropore flow parameters and macropore network characteristics was carried out first for all soil samples (Fig. 6a), second for soil samples containing biopores(s) connected from top to bottom (Fig. 6b), and third for soil samples containing inter-aggregate macropores or disconnected biopores (Fig. 6c). Many of the X-ray CT macropore network characteristics were strongly interrelated (Fig. 6). This is because large macroporosities were associated with larger macropore surface area and better connectivity of macropores. This agrees with other past studies (e.g. Katuwal et al., 2015; Larsbo et al., 2014). Macropore mean diameter and hydraulic radius were however poorly correlated with other macropore network characteristics because of inherently different measures of macropores. Significant spearman rank order correlations were also observed between macropore flow parameters and most of the X-ray CT derived macropore network characteristics (Fig. 6). X-ray CT macroporosity was strongly correlated with macropore flow parameters for all three categories of soil samples (Fig. 6a–c). Very strong correlations were observed between minimum connected macroporosity (MCMP) and macropore flow parameters for the soil samples consisting of biopores(s) connected from top to bottom (Fig. 6b). Macropore hydraulic radius and macropore mean diameter were significantly correlated with macropore flow parameters for the soil samples associated with biopore flow (Fig. 6b), whereas poorly correlated in case of soil samples associated with matrix flow (Fig. 6c). Supporting this, Elliot et al. (2010) and Quinton et al. (2008) reported strong dependency of saturated water permeability on hydraulic radius. Both macropore global and local connectivities were poorly correlated with macropore flow parameters for the soil samples associated with biopore flow (Fig. 6b), whereas significantly correlated for the soil samples associated with matrix flow (Fig. 6c). This is quite logical as biopore flow is mainly controlled by the mean pore diameter whereas matrix flow is mainly controlled by the connectivity of pores.

HESSD
12, 12089–12120, 2015

Selected correlations were graphically displayed and analyzed with linear and power regressions (which described data best) as shown in Fig. 7. The saturated water permeability (k_w) was plotted as a function of X-ray CT macroporosity as shown in Fig. 7a. A two-branch system data trend was observed at lower X-ray CT porosity, which merges into single with the increase of macroporosity. The upper branch consists of soil samples with one or more biopores connected from top to bottom that mainly governs fluid flow (filled symbols). Samples 3 and 4 marked in Fig. 7a and shown in Fig. 2 fall under this branch. The lower branch consists of soil samples in which fluid mainly flows through inter-aggregate and textural pores. Samples 1 and 2 marked in Fig. 7a and shown in Fig. 2 fall under this branch. Significant power regressions were observed between k_w and macroporosity for both categories of soil samples independently (Fig. 7a). Both Paradelo et al. (2013) and Luo et al. (2010) found similar relationships between saturated water permeability and X-ray CT derived porosity with R^2 ranging from 0.50 to 0.60. A stronger power regression was observed, R^2 increased from 0.43 to 0.76, when k_w was plotted as a function of the minimum connected macroporosity for the soil samples associated with biopore flow (Fig. 7b, filled symbols), but this is not the case for the soil samples with matrix flow (Fig. 7b, unfilled symbols). Moderate and significant power regressions were observed between k_w and macropore mean diameter (Fig. 7c). Weak but significant power regression was observed between k_w and macropore local connectivity for only those soil samples associated with matrix flow as shown in Fig. 7d. No significant regression was observed between k_w and macropore local connectivity for the soil samples associated with biopore flow (Fig. 7d, filled symbols). An explanation would be that the Euler number on which macropore local connectivity is based does not account for continuity of the pores from top to bottom.

Air permeability at −30 cm matric potential ($k_a - 30$) was plotted as a function of macroporosity as shown in Fig. 7e. Significant strong power regressions were observed for the two-branch system (Fig. 7e). Similar to k_w, power regression was significantly improved (R^2 increased from 0.49 to 0.80) when $k_a - 30$ was plotted as a function of

HESSD
12, 12089–12120, 2015

minimum connected macroporosity for the soil samples associated with biopore flow (Fig. 7f, filled symbols). A significant power regression was observed between $k_a - 30$ and macropore mean diameter for the soil samples with biopore flow while no significant regression was observed between $k_a - 30$ and macropore mean diameter for the soil samples with matrix flow (Fig. 7g). Contrary to this, significant power regression was observed between $k_a - 30$ and macropore local connectivity for soil samples associated with matrix flow while no significant regression was observed for soil samples associated with biopore flow (Fig. 7h). Similar power regressions were also observed for $k_a - 100$ as a function of macroporosity, minimum connected macroporosity, macropore mean diameter, and macropore local connectivity as shown in Fig. 7i–l, respectively.

Figure 7m and n showed significant power regressions when gas diffusivity at −30 cm matric potential ($D_P/D_0 - 30$) was plotted against macroporosity and minimum connected macroporosity, respectively. Independent significant power regressions observed for soil samples associated with biopore flow and matrix flow reflects that preferential diffusive flow occurred at −30 cm matric potential. However at −100 cm matric potential, a single regression significantly described both types of data associated with biopore flow and matrix flow as shown in Fig. 7q and r. This reflects that no preferential diffusive flow occurs at and below −100 cm matric potentials. Both $D_P/D_0 - 30$ and $D_P/D_0 - 100$ showed insignificant regressions when plotted as a function of macropore mean diameter for both categories of soil samples (Fig. 7o and s). Significant power regressions were observed when $D_P/D_0 - 30$ and $D_P/D_0 - 100$ were plotted as a function of macropore local connectivity for both soil samples associated with matrix flow and biopore flow (Fig. 8p and t). This is logical as D_P/D_0 is a concentration-driven gas transport parameter and is mainly controlled by total air-filled pore space and its connectivity, and not by the pore size (Moldrup et al., 2000).

HESSD
12, 12089–12120, 2015

4 Conclusions and perspective

1. Soil textural properties showed small spatial variability across the study site with a CV < 10 %. Despite of this, macropore flow parameters showed large spatial variability across the field with a CV > 100 %.

2. Predictive performance of empirical models/pedotransfer functions for both water and air permeabilities was quite poor at the field scale. The tested empirical model for prediction of gas diffusivity performed well at −100 cm matric potential, while failed at −30 cm matric potential particularly for the soil samples containing biopores connected from top to bottom.

3. Most of the image segmentation methods whether locally adaptive or global performed well and in a similar way. This is because the image quality was quite good in this study, i.e. with less noise and relatively clear separate peaks of the histogram associated with the soil pore and solid phases.

4. Strong correlations were observed between X-ray CT macropore network characteristics and macropore flow parameters. Minimum connected macroporosity better predicted macropore flow as compared to total macroporosity for the samples with biopore flow, and vice versa for the samples with matrix flow. Macropore mean diameter better predicted macropore flow for the samples with biopore flow, whereas macropore local connectivity better predicted macropore flow for the samples with matrix flow.

Rapid development in image analysis together with computational fluid dynamics made it possible to simulate the dynamics of flow and transport directly on X-ray CT images. One method particularly suitable for simulating macropore flow and transport on the X-ray CT images is the lattice Boltzmann method (LBM). Most of the studies to date on simulating flow and transport on X-ray CT images using LBM were based on either granular porous media (glass beads/sand) or rock geometries, and not on real soil samples where image segmentation really suffers. Strong correlations between macropore flow parameters and X-ray CT derived macropore network characteristics suggests that the lattice Boltzmann simulation of flow and transport based on X-ray CT images could be a good topic for future research, which can pave the way for the establishment of digital soil physics laboratory.

Author contributions. Muhammad Naveed, Per Moldrup, Lis Wollesen de Jonge, and Marcel Schaap designed the study and wrote the manuscript. Markus Tuller and Hans-Jorg Vögel helped in X-ray CT scanning and analysis. Ramaparsad Kulkarni performed image segmentation. Further, all the authors contributed the manuscript with the comments and suggestions throughout the writing process.

Acknowledgements. The technical assistance of Stig T. Rasmussen, Bodil B. Christensen, and Michael Koppelgaard are greatfully acknowledged. The study was part of the Soil Infrastructure, Interfaces, and Translocation Processes in Inner Space (Soil-it-is) project, which is funded by the Danish Research Council for Technology and Production Sciences.

References

Bouma, J.: Comments on micro- meso- and macroporosity of soil, Soil Sci. Soc. Am. J., 45, 1244–1245, 1981.

Buckingham, E.: Contributions to our knowledge of the aerations of soils, Bur. Soil Bull. 25, US Gov. Print. Office, Washington, D.C., 1904.

Cosby, B. J., Hornberger, G. M., Clapp, R. B., and Ginn, T. R.: A statistical exploration of the relationships of soil moisture characteristics to the physical properties of soils, Water Resour. Res., 20, 682–690, 1984.

Deepagoda, C., Moldrup, P., de Jonge, L. W., Kawamoto, K., and Komatsu, T.: Density-corrected models for gas diffusivity and air permeability in unsaturated soil, Vadose Zone J., 10, 226–238, 2011.

de Jonge, L. W., Moldrup, P., Rubaek, G. H., Schelde, K., and Djurhuus, J.: Particle leaching and particle-facilitated transport of phosphorus at field scale, Vadose Zone J., 3, 462–470, 2004.

Dougherty, R. and Kunzelmann K.: Computing local thickness of 3D structures with Image J. Micros. Microanal., 13, 1678–1679, doi:10.1017/S1431927607074430, 2007.
Elliot, T. R., Reynolds, W. D., and Heck, R. J.: Use of existing pore models and X-ray computed tomography to predict saturated soil hydraulic conductivity, Geoderma, 156, 133–142, 2010.
Feldkamp, L. A., Davis, L. C., and Kress, J. W.: Practical cone-beam algorithm, J. Opt. Soc. Am. A, 1, 612–619, 1984.
Fox, G. A., Malone, R., Sabbagh, G. J., and Rojas, K.: Interrelationship of macropores and subsurface drainage for conservative tracer and pesticide transport, J. Environ. Qual., 33, 2281–2289, 2004.
Gonzalez-Sosa, E., Braud, I., Dehotin, J., Lassabatere, L., Angulo-Jaramillo, R., Lagouy, M., Branger, F., Jacqueminet, C., Kermadi, S., and Michel, K.: Impact of land use on the hydraulic properties of the topsoil in a small French catchment, Hydrol. Process., 24, 2382–2399, 2010.
Hu, W., Shao, M. A., and Si, B. C.: Seasonal changes in surface bulk density and saturated hydraulic conductivity of natural landscapes, Eur. J. Soil Sci., 63, 820–830, 2012.
Hu, Y., Feng, J., Yang, T., and Wang, C.: A new method to characterize the spatial structure of soil macropore networks in effects of cultivation using computed tomography, Hydrol. Process., 28, 3419–3431, 2014.
Iqbal, J., Thomasson, J. A., Jenkins, J. N., Owens, P. R., and Whisler, F. D.: Spatial variability analysis of soil physical properties of alluvial soils, Soil Sci. Soc. Am. J., 69, 1338–1350, 2005.
Iversen, B. V., Schjønning, P., Poulsen, T. G., and Moldrup, P.: In situ, on-site and laboratory measurements of soil air permeability: boundary conditions and measurement scale, Soil Sci., 166, 97–106, 2001.
Iversen, B. V., Børgesen, C. D., Lægdsmand, M., Greve, M. H., Heckrath, G., and Kjærgaard, C.: Risk predicting of macropore flow using pedotransfer functions, textural maps, and modeling, Vadose Zone J., 10, 1185–1195, 2011.
Jarvis, N., Koestel, J., Messing, I., Moeys, J., and Lindahl, A.: Influence of soil, land use and climatic factors on the hydraulic conductivity of soil, Hydrol. Earth Syst. Sci., 17, 5185–5195, doi:10.5194/hess-17-5185-2013, 2013.
Jarvis, N. J.: A review of non-equilibrium water flow and solute transport in soil macropores: principles, controlling factors and consequences for water quality, Eur. J. Soil Sci., 58, 523–546, doi:10.1111/j.1365-2389.2007.00915.x, 2007.

HESSD
12, 12089–12120, 2015

Jarvis, N. J., Moeys, J., Hollis, J. M., Reichenberger, S., Lindahl, A. M. L., and Dubus, I. G.: A conceptual model of soil susceptibility to macropore flow, Vadose Zone J., 8, 902–910, doi:10.2136/vzj2008.0137, 2009.
Jassogne, L., McNeill, A., and Chittleborough, D.: 3D visualization and analysis of macro- and meso-porosity of the upper horizons of sodic, texture-contrast soil, Eur. J. Soil Sci., 58, 589–598, doi:10.1111/j.1365-2389.2006.00849.x, 2007.
Katuwal, S., Nørgaard, T., Moldrup, P., Lamandé, M., Wildenschild, D., and de Jonge, L. W.: Linking air and water transport in intact soils to macropore characteristics inferred from X-ray computed tomography, Geoderma, 237–238, 9–20, doi:10.1016/j.geoderma.2014.08.006, 2015.
Kawamoto, K., Moldrup, P., Schjønning, P., Iversen, B. V., Komatsu, T., and Rolston, D. E.: Gas transport parameters in the vadose zone: development and test of power-law models for air permeability, Vadose Zone J., 5, 1205–1215, 2006.
Klute, A. and Dirksen, C.: Hydraulic conductivity and diffusivity: laboratory methods, in: Methods of Soil Analysis, Part 1. Physical and Mineralogical Methods, 2nd Edn., edited by: Klute, A., ASA-SSSA, Madison, WI, 687–734, 1986.
Kulkarni, R., Tuller, M., Fink, W., and Wildenschild, D.: Three-dimensional multiphase segmentation of X-ray CT data of porous materials using a Bayesian Markov random field framework, Soil Sci. Soc. Am. J., doi:10.2136/vzj2011.0082, 2012.
Larsbo, M., Koestel, J., and Jarvis, N.: Relations between macropore network characteristics and the degree of preferential solute transport, Hydrol. Earth Syst. Sci., 18, 5255–5269, doi:10.5194/hess-18-5255-2014, 2014.
Lilly, A., Nemes, A., Rawls, W. J., and Pachepsky, Y. A.: Probabilistic approach to the identification of input variables to estimate hydraulic conductivity, Soil Sci. Soc. Am. J., 72, 16–24, 2008.
Luo, L., Lin, H., and Schmidt, J.: Quantitative relationships between soil macropore characteristics and preferential flow and transport, Soil Sci. Soc. Am. J., 74, 1929–1937, 2010.
Moldrup, P., Poulsen, T. G., Schjønning, P., Olsen, T., and Yamaguchi, T.: Gas permeability in undisturbed soils: measurements and predictive models, Soil Sci., 163, 180–189, 1998.
Moldrup, P., Olesen, T., Gamst, J., Schjønning, P., Yamaguchi, T., and Rolston, D. E.: Predicting the gas diffusion coefficient in repacked soil: water induced linear reduction model, Soil Sci. Soc. Am. J., 64, 1588–1594, 2000.

HESSD
12, 12089–12120, 2015

Moustafa, M. M.: A geostatistical approach to optimize the determination of saturated hydraulic conductivity for large-scale subsurface drainage design in Egypt, Agr. Water Manage., 42, 291–312, doi:10.1016/S0378-3774(99)00042-6, 2000.
Naveed, M.: Revealing soil architecture and quality: linking state-of-the-art soil biophysicochemical measurements, visualizations, and simulations, PhD thesis, Aarhus University, Aarhus, 2014.
Naveed, M., Moldrup, P., Arthur, E., Wildenschild, D., Eden, M., Lamande, M., Vogel, H.-J., and de Jonge, L. W.: Revealing soil structure and functional macroporosity along a clay gradient using X-ray computed tomography, Soil Sci. Soc. Am. J., 77, 403–411, 2013.
Naveed, M., Moldrup, P., Arthur, E., Holmstrup, M., Nicolaisen, M., Tuller, M., Herath, L., Hamamoto, S., Kawamoto, K., Komatsu, T., Vogel, H.-J., and de Jonge, L. W.: Simultaneous loss of soil biodiversity and functions along a copper contamination gradient: when soil goes to sleep, Soil Sci. Soc. Am. J., 78, 1239–1250, doi:10.2136/sssaj2014.02.0052, 2014a.
Naveed, M., Moldrup, P., Vogel, H.-J., Lamandé, M., Wildenschild, D., Tuller, M., and de Jonge, L. W.: Impact of long-term fertilization practice on soil structure evolution, Geoderma, 217–218, 181–189, 2014b.
Norgaard, T., Moldrup, P., Olesen. P., Vendelboe, A. L., Iversen, B. V., Greve, M. H., Kjaer, J., and de Jonge, L. W.: Comparative mapping of soil physical-chemical and structural parameters at field scale to identify zones of enhanced leaching risk, J. Environ. Qual., 42, 271–283, 2013.
Otsu, N.: A threshold selection method from gray-level histograms, Automatica, 11, 23–27, 1975.
Paradelo, M., Moldrup, P., Arthur, E., Naveed, M., Holmstrup, M., López-Periago, J. E., and de Jonge, L. W.: Effects of Past Copper Contamination and Soil Structure on Copper Leaching from Soil, J. Environ. Qual., 42, 1852–1862, doi:10.2134/jeq2013.05.0209, 2013.
Pérèsa, G., Bellidoa, A., Curmib, P., Marmonierc, P., and Cluzeaua, D.: Relationships between earthworm communities and burrow numbers under different land use systems, Pedobiologia, 54, 37–44, 2012.
Quinton, W. L., Hayashi, M., and Carey, S. K.: Peat hydraulic conductivity in cold regions and its relation to pore size and geometry, Hydrol. Process., 22, 2829–2837, 2008.
Raczkowski, C. W., Mueller, J. P., Busscher, W. J., Bell, M. C., and McGraw, M. L.: Soil physical properties of agricultural systems in a large-scale study, Soil Till. Res., 119, 50–59, 2012.

Rasband, W. S.: Image-J., US National Institutes of Health, Bethesda, Maryland, USA, available at: http://imagej.nih.gov/ij/ (last access: 19 April 2014), 2011.
Revil, A. and Cathles, L. M.: Permeability of shaly sands, Water Resour. Res., 35, 651–662, 1999.
Ridler, T. and Calvard, S.: Picture thresholding using an iterative selection method, IEEE Trans. Syst. Man Cybern., 8, 630–632, doi:10.1109/TSMC.1978.4310039, 1978.
Sauvola, J. and Pietikainen, M.: Adaptive document image binarization, Pattern Recogn., 33, 225–236, doi:10.1016/S0031-3203(99)00055-2, 2000.
Schaap, M. G., Leij, F. L., and van Genuchten, M. T.: Rosetta: a computer programme for estimating soil hydraulic parameters with hierarchical pedotransfer functions, J. Hydrol., 251, 163–176, 2001.
Schjønning, P., Eden, M., Moldrup, P., and de Jonge, L. W.: Two-chamber, two-gas and onechamber, one-gas methods for measuring the soil-gas diffusion coefficient: validation and inter-calibration, Soil Sci. Soc. Am. J., 77, 729–744, doi:10.2136/sssaj2012.0379, 2013.
Sharma, P., Shukla, M. K., and Mexal, J. G.: Spatial variability of soil properties in agricultural fields of Southern New Mexico, Soil Sci., 176, 288–302, 2011.
Udawatta, R. P., Anderson, S. H., Gantzer, C. J., and Garrett, H. E.: Influence of prairie restoration on CT-measured soil pore characteristics, J. Environ. Qual., 37, 219–228, 2008.
USDA-NRCS Web Soil Survey, available at: websoilsurvey.nrcs.usda.gov/app/WebSoilSurvey.aspx, 2010.
Vereecken, H., Maes, J., Feyen, J., and Darius, P.: Estimating the soil moisture retention characteristic from texture, bulk density, and carbon content, Soil Sci., 148, 389–403, 1989.
Vereecken, H., Weynants, M., Javaux, M., Pachepsky, Y., Schaap, M. G., and van Genuchten, M. T.: Using pedotransfer functions to estimate the van Genuchten–Mualem soil hydraulic properties: a review, Vadose Zone J., 9, 795–820, 2010.
Vogel, H.-J.: A numerical experiment on pore size, pore connectivity, water retention, permeability, and solute transport using network models, Eur. J. Soil Sci., 51, 99–105, 2000.
Vogel, H.-J., Weller, U., and Schluter, S.: Quantification of soil structure based on Minkowski functions, Comput. Geosci., 36, 1236–1245, doi:10.1016/j.cageo.2010.03.007, 2010.
Wang, Y., Shao, M., Liu, Z., and Horton, R.: Regional-scale variation and distribution patterns of soil saturated hydraulic conductivities in surface and subsurface layers in the loessial soils of china, J. Hydrol., 487, 13–23, 2013.

HESSD
12, 12089–12120, 2015

Wildenschild, D. and Sheppard, A.: X-ray imaging and analysis techniques for quantifying pore-scale structure and processes in subsurface porous medium systems, Adv. Water Resour., 51, 217–246, 2013.
Wosten, J. H. M., Lilly, A., Nemes, A., and Bas, C. L.: Development and use of a database of hydraulic properties of European soils, Geoderma, 90, 169–185, 1999.

HESSD
12, 12089–12120, 2015

Table 1. Descriptive statistics for selected soil physical properties ($n = 65$).

Variable	Minimum	Maximum	Mean	Median	SD	Skewness	CV %
Clay (g 100 g^{-1})	14.18	18.93	15.82	15.54	1.36	0.65	9
Silt (g 100 g^{-1})	23.30	33.32	30.12	30.10	1.66	−1.21	6
Sand (g 100 g^{-1})	44.89	59.00	50.71	50.72	2.14	0.32	4
Organic matter (g 100 g^{-1})	2.90	3.75	3.35	3.38	0.20	−0.42	6
Saturated water permeability, k_w (µm^2)	0.003	118.1	12.04	0.39	26.30	2.73	218
Air permeability at −30 cm, $k_a - 30$, (µm^2)	0.03	109.19	10.87	3.21	22.33	3.03	205
Air permeability at −100 cm, $k_a - 100$, (µm^2)	0.19	151.10	14.72	5.42	27.13	3.26	184
Gas diffusivity at −30 cm, $D_P/D_0 - 30$	0.0001	0.018	0.0026	0.0017	0.003	2.74	123
Gas diffusivity at −100 cm, $D_P/D_0 - 100$	0.0004	0.025	0.0052	0.0040	0.005	2.31	92

HESSD
12, 12089–12120, 2015

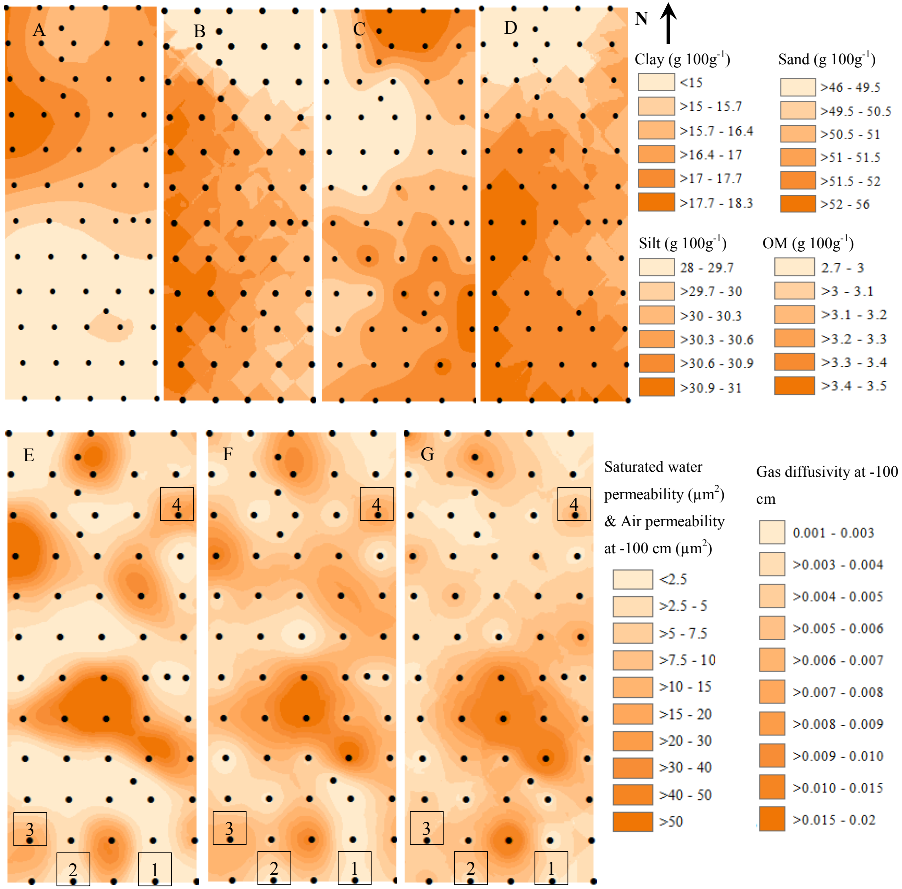

Figure 1. Contour maps for soil textural properties and macropore flow parameters, **(a)** clay (< 2µm), **(b)** silt (2–50 µm), **(c)** sand (50–2000 µm), **(d)** organic matter, **(e)** saturated water permeability (µm^2), **(f)** air permeability (µm^2) at −100 cm matric potential, and **(g)** gas diffusivity at −100 cm matric potential, marked samples are shown in Fig. 2.

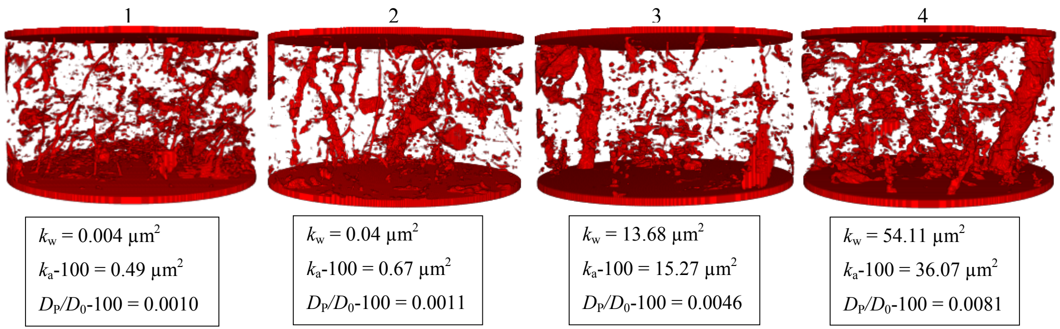

Figure 2. Example soil columns (3-D pore visualizations) and respective measured macropore flow parameters, where k_w is saturated water permeability, $k_a - 100$ and $D_P/D_0 - 100$ is air permeability and gas diffusivity at −100 cm matric potentials, respectively.

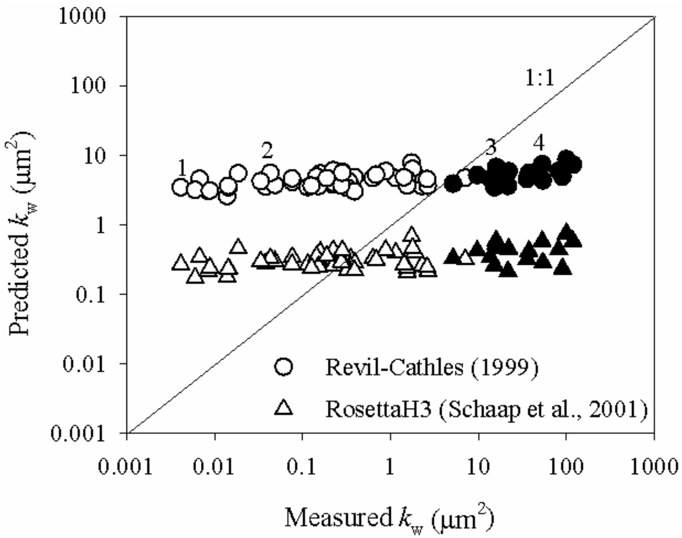

Figure 3. Performance of empirical predictive models for saturated water permeability (k_w), filled symbols represent samples with biopore flow and unfilled symbols represent samples with matrix flow, marked samples are shown in Fig. 2.

HESSD
12, 12089–12120, 2015

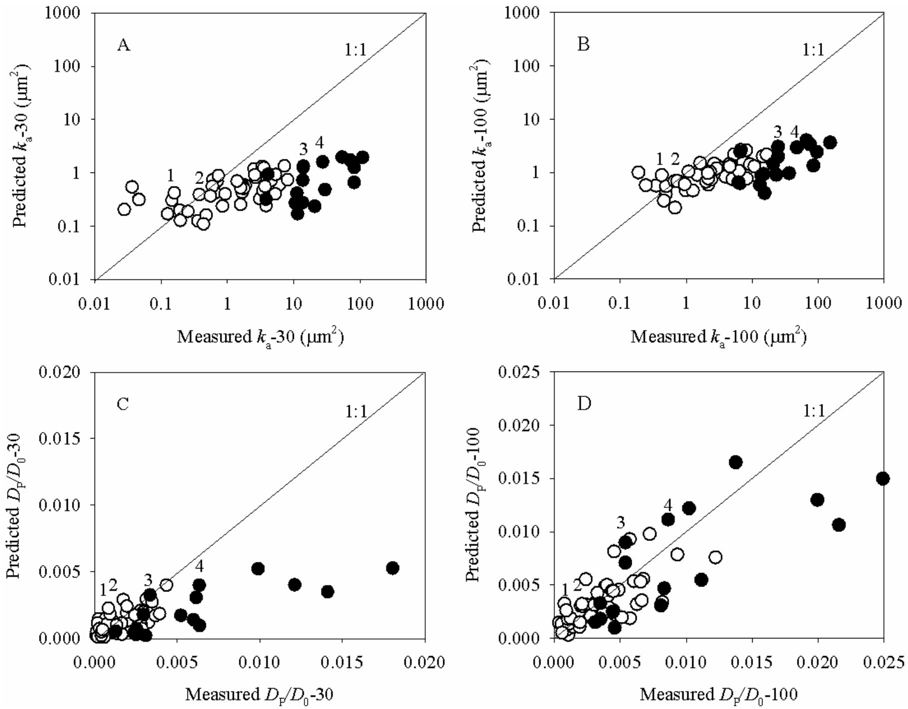

Figure 4. Performance of empirical predictive models for air permeability (k_a) and gas diffusivity (D_P/D_0) at −30 and −100 cm matric potentials. **(a)** Deepagoda et al. (2011) model, **(b)** Deepagoda et al. (2011) model, **(c)** WLR-Marshall model (Moldrup et al., 2000), and **(d)** WLR-Marshall model (Moldrup et al., 2000), filled symbols represent samples with biopore flow and unfilled symbols represent samples with matrix flow, marked samples are shown in Fig. 2.

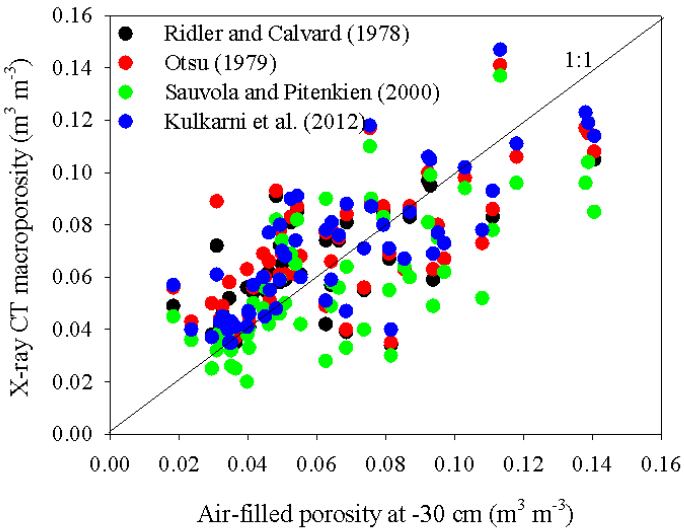

Figure 5. X-ray CT macroporosity obtained using four different segmentation methods plotted as a function of physically measured air-filled porosity at −30 cm matric potential.

HESSD
12, 12089–12120, 2015

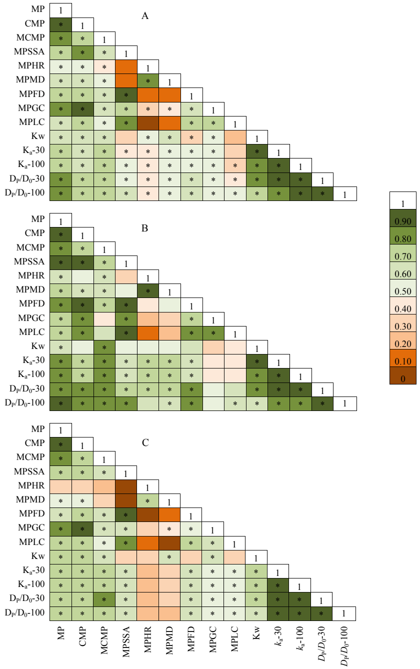

Figure 6. Spearman rank order correlation analysis **(a)** all samples ($N = 65$), **(b)** samples with biopore flow ($N = 16$), and **(c)** samples with matrix flow ($N = 49$), star indicates significant correlations at p value < 0.01; where MP is macroporosity, CMP is connected macroporosity, MCMP is minimum connected macroporosity, MPSSA is macropore specific surface area, MPHR is macropore hydraulic radius, MPMD is macropore mean diameter, MPFD is macropore fractal dimension, MPGC is macropore global connectivity, MPLC is macropore local connectivity, k_w is saturated water permeability, $k_a - 30$ is air permeability at −30 cm matric potential, $k_a - 100$ is air permeability at −100 cm matric potential, $D_P/D_0 - 30$ is gas diffusivity at −30 cm matric potential, and $D_P/D_0 - 100$ is gas diffusivity at −100 cm matric potential.

HESSD
12, 12089–12120, 2015

HESSD
12, 12089–12120, 2015

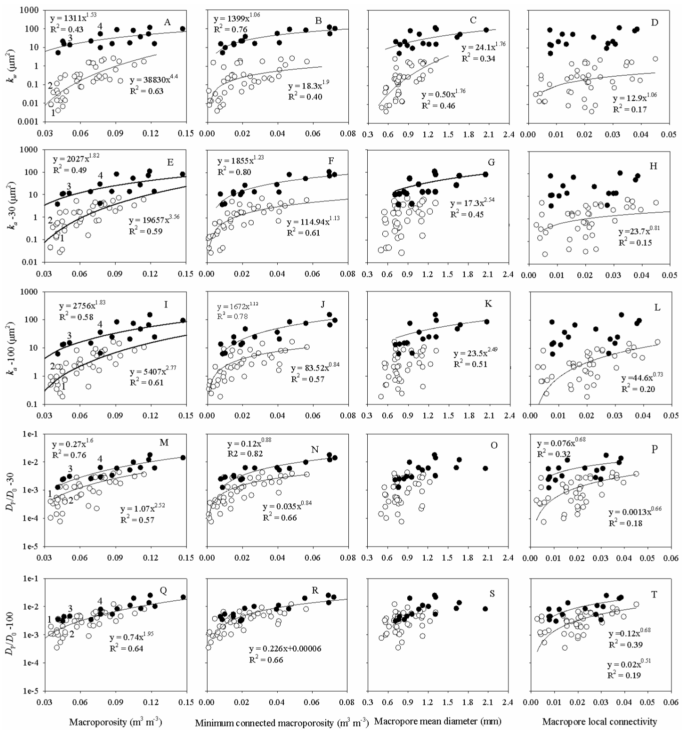

Figure 7. Saturated water permeability (k_w), air permeability at −30 cm matric potential (k_a-30), air permeability at −100 cm matric potential (k_a-100), gas diffusivity at −30 cm matric potential (D_P/D_0-30), and gas diffusivity at −100 cm matric potential (D_P/D_0-100) were plotted as a function of selected X-ray CT macropore network characteristics, filled symbols represent samples with biopore flow and unfilled symbols represent samples with matrix flow. Regressions either linear or power that best described data were fitted if significant at $p < 0.01$, two separate regressions were fitted for samples with biopore flow and matrix flow if they were significantly different.